Journal of Peptide Science, Vol. 2, 75–90 (1996)

# The Solution Structure of the Immunodominant and Cell Receptor Binding Regions of Foot-and-mouth Disease Virus Serotype A, Variant A

**MONICA PEGNA[1,2], HENRIETTE MOLINARI[2,3], LUCIA ZETTA[2], WILLIAM A. GIBBONS[4], FRED BROWN[5], DAVE ROWLANDS[6], GIULIANO SILIGARDI[4] and PAOLO MASCAGNI[1]**

[1] Department of Peptide Chemistry, Italfarmaco Research Centre, Milan, Italy
[2] NMR laboratory, Istituto delle Macromolocole, CNR, Milan, Italy
[3] Istituto Policattedra, University of Verona, Italy
[4] Department of Pharmaceutical Chemistry, School of Pharmacy, University of London, UK
[5] US Department of Agriculture, Agricultural Research Service, Plum Island Animal Disease Center, New York, USA
[6] Department of Molecular Sciences, Wellcome Foundation, UK

*Received 1 May 1995*
*Accepted 29 September 1995*

Abstract: The solution structure of a 20 amino acid long peptide corresponding to the region 141–160 of the envelope protein Vp1 from foot-and-mouth disease virus (FMDV) serotype A, variant A, has been determined by a combination of NMR experiments and computer calculations. The peptide contains both the immunodominant epitope as well as the sequence (RGD) used by the virus to bind the cell receptor in the initial stages of infection. These two sites have been shown to partially overlap.

One hundred and thirty-five NMR distance constraints were used to obtain a set of 11 structures by distance geometry, minimization and molecular dynamics simulations. These structures were divided into two homogeneous families based upon backbone superimposition. The first and most populated family was characterized by a backbone RMS of $1.5 \pm 0.4$ Å, the second by a backbone RMS of $0.8 \pm 0.2$ Å. The two families had similar structural features and differed mainly in the backbone angles of G149. In the larger of the two families these angles favoured the formation of a loop comprising residues 147 to 152 and stabilized by a H-bond between the NH of D147 and the CO of A152. In the second family, where this bond was absent, the peptide adopted in this region the shape of an irregular helix. The C-terminal half of the peptide (152–159) was similar in both families and largely helical. Similar structural features were also found within the VRGDS sequence (144–148) which was assigned to a $\beta$-turn type IV. The features of the two families of structures were found to be different from those of the recently published X-ray structure of the antigenic loop of a chemically modified form of FMDV. Proposals accounting for these differences are provided which take into account the dual activity of the 141–160 sequence (i.e. antibody binding and cell invasion through receptor binding).

Keywords: FMDV; structure; NMR spectroscopy; NOE constraints; RGD (Arg-Gly-Asp)

Address for correspondence: Paolo Mascagni, Department of Peptide Chemistry, Italfarmaco Research Centre, Via Lavoratori 54, Cinisello-Balsamo, 20092 Milan, Italy; Tel. 39-2-6443-3090, Fax: 39-2-6601-1579.


CCC 1075-2617/96/020075-16

## INTRODUCTION

Foot-and-mouth disease virus (FMDV) is the cause of an economically important disease afflicting domestic livestock. The disease can be prevented by vaccination but the preparation of appropriate vaccines is complicated by the occurrence of seven distinct serotypes of the virus. A vaccine prepared from a virus of an individual serotype does not provide any protection against infection with viruses of the other six serotypes. In addition, there is considerable antigenic variation within the individual serotypes so that a vaccine prepared from an isolate may not provide protection against other isolates of the same serotype. Consequently an understanding of the structural basis for this variation could lead to the development of vaccines with a broader antigenic spectrum.

The major immunogen in virus harvests is the intact virus particle. This is an icosahedral particle, 30 nm in diameter, consisting of one molecule of single-stranded RNA surrounded by a capsid comprising 60 molecules each of four proteins, VP1–VP4. Stepwise dissection of the particle has led to the identification of the immunodominant site within residues 141–160 of VP1. Peptides corresponding to this sequence are highly immunogenic and can provide protective immunity in experimental animals [1]. This sequence also contains residues RGD at positions 145–147, a triplet known to be a recognition element in many integrin-dependent cell adhesion processes and to be implicated in the attachment of FMDV to its cell receptor [2]. In addition there is evidence to suggest that the cell receptor binding region on the virus includes at least part of the antigenic determinant [3].

X-ray diffraction studies with viruses of both serotype O [4] and serotype C [5] have shown that the immunogenic site is located within an exposed and highly flexible loop (the G–H loop). However, the coordinates for this loop could not be determined except for serotype O under reducing conditions, which eliminated a disulphide bond between C134 of VP1 and C130 of VP2 [6]. Of the seven serotypes of the virus, only those of serotype O have the potential to form a disulphide bond involving this loop region. Consequently studies on structure–antigenic function relationships within serotype O may not apply to the other serotypes of the virus.

The 141–160 region of VP1 is highly variable between viruses of different serotypes in both sequence and antigenicity thus providing the opportunity to reach an understanding of the structural basis for antigenic variation. A virus of serotype A, sub-type 12, has provided a valuable model for such a study because several antigenic variants have been isolated from a single source in which the capsid protein regions differed only at positions 148 and 153 of VP1 (Figure 1) [7]. The 141–160 peptides corresponding to four of these variants (called peptides A, B, C and USA) have been compared by CD spectroscopy [8, 9]. The results allowed the correlation between the serological properties of the four peptides (and viruses) with their conformational properties to be made.

In this paper and the accompanying one (p. 91) NOE constraints obtained from 2D-, 3D-, homo- and heteronuclear NMR experiments have been combined with distance geometry (DG) and restrained molecular dynamics (RMD) calculations to compare the structural features of peptides A and USA in TFE-OH solutions.

There are contrasting evidences and opinions concerning the use of TFE for structural studies on biologically relevant peptides. Thus, on one hand TFE has been widely considered as a helix inducing solvent, while on the other recent work has clearly demonstrated that it stabilized helices only in those regions of peptides that have a propensity to form helical structures [10–13]. Furthermore peptides predicted to be helical have been shown to form a helix in either SDS or alcohol-containing solutions but are found as $\beta$-strands when part of the proteins from which they were derived [14].

In the case of the peptides described here and in the accompanying paper the use of TFE was suggested by the following considerations:

(1) The CD spectra in water of peptides A, B, C and USA showed little evidence of defined secondary structure composition [8, 9].
(2) When the same peptides were studied in different solvents (i.e. TFE, MeOH, ethandiol–water mixtures) and in the presence of additives such as SDS, their CD spectra were characterized by minima in the 204–206 nm range and at 222 nm [8, 9].
(3) The CD spectra in TFE of peptides A and C were similar and different from those of B and USA. The latter were in turn similar to each other. This classified the four peptides in the same two classes (i.e. A with C and B with USA), deduced from their serological behaviour. Similar conclusions were reached when the helix-forming properties of seven antigenic variants of serotype A-12 studied by CD in TFE were shown to correlate well with their serological cross-reactivity [15].

141-142-143-144-145-146-147-**148**-149-150-151-152-**153**-154-155-156-157-158-159-160

Gly-Ser-Gly-Val-Arg-Gly-Asp-**Phe**-Gly-Ser-Leu-Ala-**Pro**-Arg-Val-Ala-Arg-Gln-Leu-Pro (USA)

Gly-Ser-Gly-Val-Arg-Gly-Asp-**Ser**-Gly-Ser-Leu-Ala-**Leu**-Arg-Val-Ala-Arg-Gln-Leu-Pro (A)

Gly-Ser-Gly-Val-Arg-Gly-Asp-**Leu**-Gly-Ser-Leu-Ala-**Pro**-Arg-Val-Ala-Arg-Gln-Leu-Pro (B)

Gly-Ser-Gly-Val-Arg-Gly-Asp-**Ser**-Gly-Ser-Leu-Ala-**Ser**-Arg-Val-Ala-Arg-Gln-Leu-Pro (C)

Figure 1 Amino acid sequence of the 141–160 region of four antigenic variants (A, B, C and USA) of FMDV, serotype A, sub-type 12, strain 119. The four peptides differ for two residues, those at positions 153 and 148. In this paper the residues were numbered from 1 to 20.

Thus, it was reasoned, the combined use of TFE and NMR studies should allow a more detailed investigation into the structural differences between these two pairs of peptides and made a correlation with their biological behaviour possible.

## MATERIALS AND METHODS

### Materials

The peptide was synthesized as a carboxyamide derivative on a solid support (MBHA resin) using t-BOC chemistry. After HF cleavage the peptide was purified by RP-HPLC (purity > 97%) and characterized by FAB-MS (expected 1994; found M + H 1995).

$CF_3-CD_2-OH$ (TFE-d2) was obtained by distillation of a 1 : 1 (v/v) mixture of $CF_3-CD_2-OD$ (Cambridge Isotope Ltd, Cambridge, UK) and $H_2O$. The fractions used for the NMR experiments had boiling points ranging from 73 to 75 °C.

### Proton NMR Experiments

NMR spectra were obtained on a Bruker AM-500 spectrometer, using 2 mM samples of peptide. Total correlation spectroscopy (clean-TOCSY) [16] with a spin-lock of 80 ms using 16 cycles of a MLEV-17 sequence was used to assign the proton spectrum. Suppression of the solvent resonance was achieved by coherent presaturation. To determine the peptide secondary structure, NOESY experiments with variable mixing times (200–450 ms) were used. All 2D experiments were recorded with 2048 data points in $t_2$ and 512 $t_1$ increments, with a spectral width of 6024 Hz in both dimensions. In the NOESY experiments, the solvent signal was suppressed with presaturation during the relaxation delay of 2 s. The NMR data were processed both on a Bruker X32 station using UXNMR and AURELIA (Bruker) and on an IRIS 3D-30 computer using Felix (Biosym).

### Molecular Modelling

DG, EM and RMD calculations [17–22] were carried out using DGII (Biosym) and DISCOVER (Biosym) respectively. In all computer calculations, performed on a Personal IRIS 3D-30, 135 distances were included as restraints.

Initial structures were obtained from NOE data via distance geometry calculations based on the 'embed'

algorithm. Using the experimentally derived distances and those implicit in the primary sequence of the peptide, i.e. covalent bond lengths and bond angles, a bond matrix was prepared which was subsequently smoothed using triangle and inverse triangle inequalities and successively 'embedded' in 3D space. The resulting structures were refined to minimize a 'penalty function' which is a measurement of the deviation between distances/information in the structure and the bound matrix. The DG calculations also included a simulated annealing procedure which imposed an upper bound $T_{max}$ (300 K) on the temperature and was gradually reduced to zero.

The DG structures were first subjected to 1000 steepest descent EM steps, then to 5000 conjugate gradient and to 5000 'Lennard-Jones' steps. A convergence criterion of 0.01 as maximum derivative was used. The distance restraint force constant $k_{res}$ was 10 kcal $mol^{-1}$ $A^{-2}$ and a distance-dependent dielectric constant $\varepsilon = r$ was used. An average decrease in energy of 87% was obtained.

For RMD simulations the time step was $\Delta t = 0.001$ ps, and the cut-off radius for non-bonded interactions 1 nm. The RMD refinement time was 50 ps, with a distance restraint force constant of 10 kcal $mol^{-1}$ $A^{-2}$ and a distance-dependent dielectric constant. Finally the kinetic energy was removed from the system by another cycle of steepest descent and conjugate gradient energy minimization using the same value for the force constant. A new decrease in potential energy of 7% was thus obtained, while average restraint violations were slightly increased.

## RESULTS

Conformational averaging is a common problem in the conformational analysis of linear peptides. Unless the conformational freedom is restricted (e.g. disulphide bonds), the NMR parameters such as NOEs, defining the conformational space, are the average over all conformers present and their interpretation is not straightforward.

In the case of the peptide described here our previous CD studies showed a difference in helical and $\beta$-turn content of 4% and −1% respectively between the spectrum in TFE at room temperature (r.t.) and that at −30 °C where the peptide was in a stabilised conformation [8, 9]. Based on these data it seemed therefore reasonable to assume that, although peptide A was in TFE and at r.t., experiencing conformational averaging, this was probably restricted enough so as to make structural studies

Table 1 $^1$H Chemical Shifts (p.p.m.) of Peptide A in TFE at 305 K

| Residue | NH | $\alpha_{CH}$ | $\beta_{CH}$ | $\gamma_{CH}$ | Other |
|---|---|---|---|---|---|
| G1 | | | | | |
| S2 | 8.30 | 4.57 | 3.96/4.05 | | |
| G3 | 8.18 | 4.08/4.00 | | | |
| V4 | 7.65 | 4.10 | 2.17 | 1.04 | $^{\delta}$CH = 3.26 |
| R5 | 7.93 | 4.36 | 1.98/1.90 | 1.77/1.73 | $^{\epsilon}$CH = 7.14 |
| G6 | 8.04 | 4.00/4.00 | | | |
| D7 | 8.17 | 4.82 | 2.97 | | |
| S8 | 8.19 | 4.34 | 4.10/4.08 | | |
| G9 | 8.28 | 4.02/3.98 | | | |
| S10 | 7.84 | 4.34 | 4.12/4.04 | | |
| L11 | 7.74 | 4.23 | 1.82 | 1.82 | $^{\delta}$CH = 1.02/0.96 |
| A12 | 7.79 | 4.10 | 1.54 | | |
| L13 | 7.61 | 4.19 | 1.89/1.70 | 1.80 | $^{\delta}$CH = 1.00/0.96 |
| R14 | 7.71 | 4.17 | 2.07 | 1.88/1.77 | $^{\delta}$CH = 3.24 |
| | | | | | $^{\epsilon}$CH = 7.01 |
| V15 | 8.04 | 3.87 | 2.24 | 1.10/1.02 | |
| A16 | 8.08 | 4.21 | 1.56 | | |
| R17 | 7.70 | 4.36 | 2.07/1.98 | 1.86 | $^{\delta}$CH = 3.26 |
| | | | | | $^{\epsilon}$CH = 7.04 |
| Q18 | 7.92 | 4.38 | 2.29/2.23 | 2.47 | |
| L19 | 7.57 | 4.76 | 1.80/1.59 | 1.84 | $^{\delta}$CH = 1.01 |
| P20 | - | 4.46 | 2.30/2.07 | 2.13 | $^{\delta}$CH = 3.87/3.66 |

Table 2 Vicinal Coupling Constants (296 K) and Temperature Coefficients of Peptide A in TFE

| Residue | $J_{NH-\alpha}$(Hz) | $\Delta\delta_{NH}/\Delta T$/(p.p.b) |
|---|---|---|
| Gly 1 | | |
| Ser 2 | 6.9 | 4.8 |
| Gly 3 | – | 5.0 |
| Val 4 | 6.9[a] | 4.9 |
| Arg 5 | 6.2 | 6.7 |
| Gly 6 | – | 4.9 |
| Asp 7 | 6.6 | 4.7 |
| Ser 8 | – | 6.6 |
| Gly 9 | – | 4.8 |
| Ser 10 | 4.9 | 2.9 |
| Leu 11 | 4.6 | 2.8 |
| Ala 12 | 2.6[a] | 3.4 |
| Leu 13 | 4.9[a] | 2.6 |
| Arg 14 | 6.6[a] | 2.2 |
| Val 15 | 5.6 | 6.0 |
| Ala 16 | 3.3[a] | 5.6 |
| Arg 17 | 6.6 | 4.2 |
| Gln 18 | 7.9 | 2.4 |
| Leu 19 | 7.5[a] | 3.4 |
| Pro 20 | – | – |

[a] Vicinal coupling constants at 300 K.

using NOE constraints meaningful. The results described here which indicate that homogenous structures were obtained from the combination of NMR parameters and computer simulations seem to justify this assumption.

NMR spectra were recorded at r.t. in TFE-d2 at a peptide concentration of 2 mM which previous CD studies had indicated did not give rise to aggregation.

### Assignments of the Proton Spectrum

The majority of sequence-specific and sequential NMR assignments (Table 1) were obtained by a combination of homonuclear 2D-NMR experiments at 500 MHz, following the standard strategy for small proteins [23]. $J_{N\alpha}$-coupling constants were measured directly from 1D spectra at different temperatures. The results from these assignments are shown in Figures 2(a), 2(b) and 3 and Tables 1 and 2.

### Internuclear Distance Evaluation from NMR Data

In the accompanying paper the correlation time $\tau_c$ for peptide USA was calculated from $^{13}C$–$^{1}H$ heteronuclear 2D experiments and found to be 0.9 ns. This was used together with the results from NOE effects measured at mixing times ranging between 200 and 450 ms to conclude that the influence of spin diffusion on the NOE intensities was negligible [24].

Since peptide A was identical in size to peptide USA and highly homologous to the latter it was felt that the same correlation time of 0.9 ns could also apply to this peptide. Average interproton distances were thus measured with the initial rate approximation method [23] and the results obtained shown in Figure 4.

### NMR Temperature Studies

1D spectra of peptide A in TFE-$d_2$ solutions were recorded in the temperature range 290–320 K and at temperature intervals of 5 K. To avoid ambiguities in the assignment of the NH resonances, clean-TOCSY experiments were carried out at the two extreme temperatures studied.

Of the 18 temperature coefficients thus measured (Table 2), 7 had values smaller than 4 p.p.b./K (S10, L11, A12, L13, R14, Q18 and L19) and were assigned to either hydrogen-bonded or solvent-shielded NHs. Conversely 2 residues (R5 and S8) had temperature coefficients larger than 6 p.p.b./K and hence were solvent exposed. The remaining values (S2, G3, V4, G6, D7, G9, V15, A16, R17) ranged from 4.2 to 6 and might reflect less tight hydrogen bonds.

### Patterns of NMR Data Indicating the Presence of Regular Secondary Structures

2D NOESY $NH_i$–$NH_{i+1}$ cross-peaks (Figures 2(b) and 3) were found between all residues in the range G3–L11. The only exceptions were the NH7–NH8, NH11–NH12 and NH15–NH16 NOEs which, although potentially present, could not be unambiguously assigned owing to signal overlaps. These NOEs established a continuity in the $d_{NN}$ connectivity network, which was reminiscent of helical structures [23]. This conclusion was supported by $\alpha CH_i$–$\beta CH_{i+3}$ and $\alpha_i$–$N_{i+n}$ cross-peaks, also typical of helices, which were found in the 4–18 region and in all cases where the assignment was unique (see below).

In the region 4–8 the following NOEs were found: NH4–NH5; NH5–NH6; NH6–NH7; α4–NH5; α5–NH6; α7–NH8; α3–NH5; α4–β7; α5–β7 (Figures 2–4). Neither these correlations nor the $NH_i$–$NH_{i+1}$ NOEs (Figures 3 and 4) could be used to identify defined secondary structure elements involving the RGD sequence. However a temperature coefficient of 4.7 p.p.b./K found for the NH of D7 which contrasted with the larger value of 6.6 p.p.b./K for residue S8, suggested the existence of a turn possibly stabilized by an H-

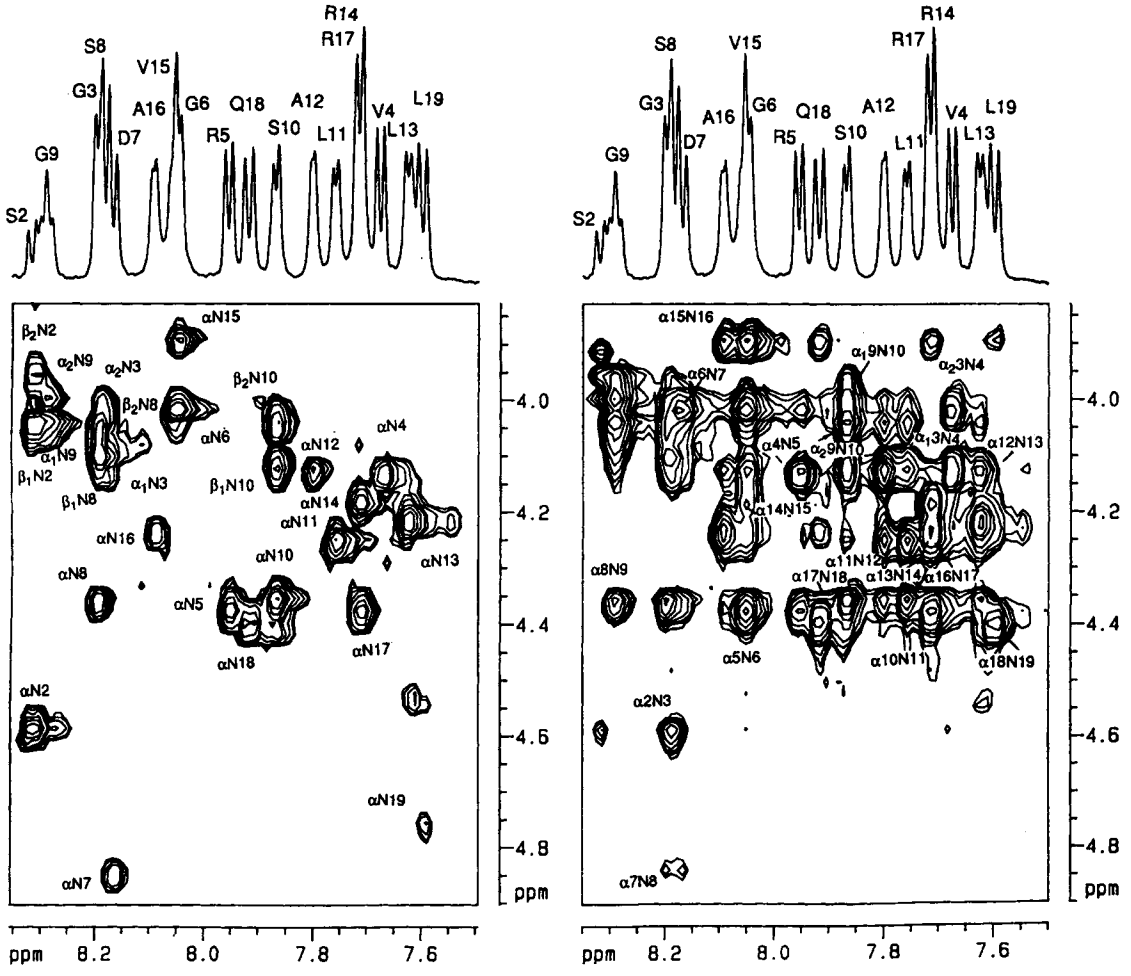


Figure 2 $^1$H-NMR spectra of peptide A (2 mM) in TFE-$d_2$ at 305 K. NH-C$\alpha$H region of: clean-TOCSY (a) and NOESY (b). The spectral width was 6024 Hz and 512 $t_1$ increments were implemented over 2048 points in $t_2$ dimension. Data matrix was zero filled to 1024 in $F_1$ and a $\pi/2$ shifted sine-bell window was applied in both dimensions. The isotropic mixing and the mixing times were 80 and 450 ms respectively, used for the two sequences.

bond between residues 4 and 7. Different types of turns have been identified in RGD containing peptides. For instance, a $\beta$-turn type II has been recently [25] assigned to the YGRGDSP peptide whilst a $\beta$-turn type VII has been proposed for a cyclic CRGDC peptide [26]. Furthermore molecular simulation calculations using a model FMDV peptide pointed to the presence of two consecutive $\gamma$-turns [27].

Several NOEs (i.e. $NH_i$-$NH_{i+1}$, $\beta_i$-$NH_{i+1}$, $\alpha$9–$\beta$12, $\alpha$12–$\beta$15, $\alpha$14–$\beta$17, $\alpha$12–N15, $\alpha$15–N18 and $\alpha$12–N16) found in the C-terminal half of the peptide indicated the existence of a helical structure. In agreement with this conclusion were (1) analysis of secondary chemical shifts of the C$\alpha$ protons (see Table 1), (2) the NH temperature coefficients which, with the excep-

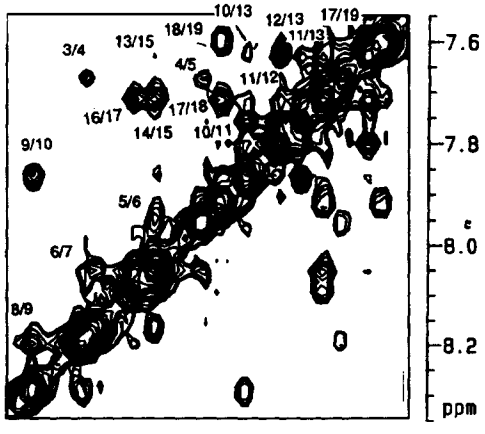


Figure 3 Amide region of the 2D NOESY spectrum of peptide A in TFE-$d_2$ solutions at 305 K.

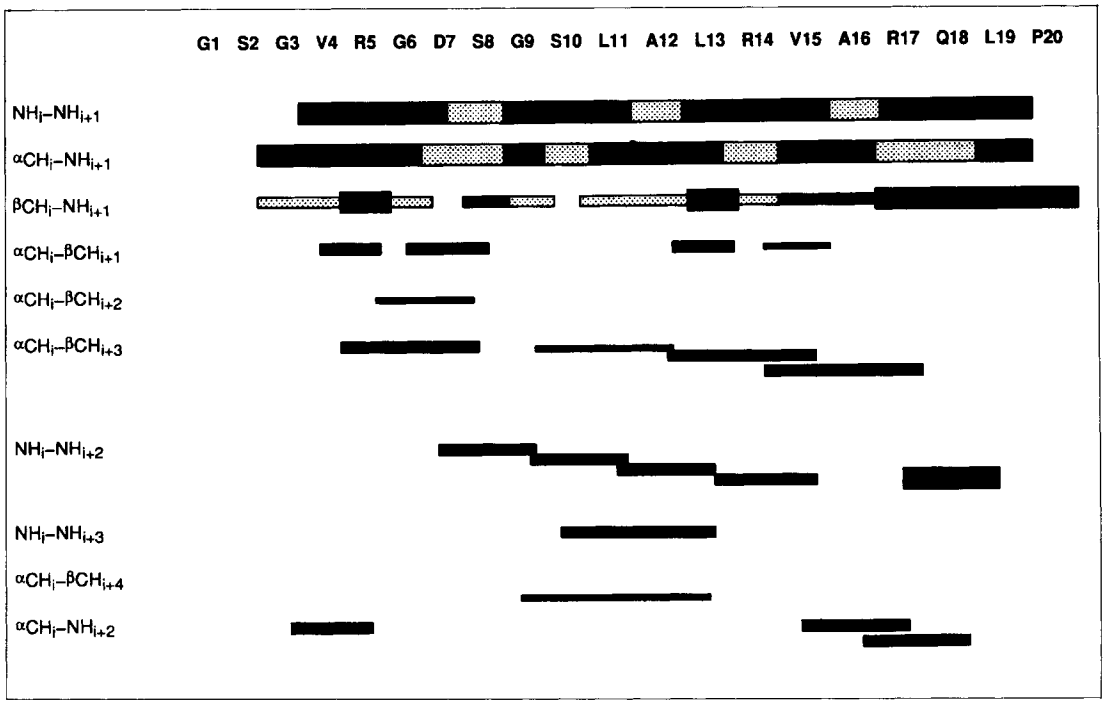


Figure 4 Summary of main chain NOE connectivities. Gray areas of sequential NOEs indicate the presence of more then one overlapping peak. Strong, medium and weak NOEs are represented by lines of different thickness. Some long-range (about 20) backbone–side chain and side chain–side chain connectivities are not shown for clarity reasons.

tion of V15, A16 and R17 (Table 2), were less than 3.5 p.p.b./K and (3) $J_{N\alpha}$-coupling constants of residues 10 to 16, which ranged from 2.6 to 4.9 Hz, residues 14 and 15 being the only exceptions (Table 2).

## Molecular Modelling

One hundred and thirty-five distance constraints were derived from NMR data. Of these, 81 were interresidue, divided in 36 backbone–backbone constraints, 42 backbone–sidechain and 3 sidechain–sidechain constraints. The whole set of NOE constraints was used to generate 100 structures by distance geometry. H-bonds and $J$-coupling constants were not used as constraints.

Most of the structures thus calculated had small restraint energies and high potential energies. Application of EM calculations reduced the latter considerably. Eleven structures were selected which had values of potential energy within 20 kcal of the structure with the lowest energy and an average distance violation [28] $\langle r_{viol} \rangle$ of less than 0.2 Å. RMD simulations over 50 ps and at 300 K were performed on the selected structures. Restraints were used with lower and upper bounds, to take averaging effects into account. The potential energies before and after dynamics are shown in Table 3 together with $\langle r_{viol} \rangle$. The restraint contribution in energy to the global force field was less than 10% of the total energy. Backbone $\phi$ and $\psi$ angles for the 2–19 residues were inside allowed regions of the Ramachandran plot (Table 4). Table 5 contains an analysis of the backbone H-bonds found in the 11 structures. Only those H-bonds found in at least four structures are shown.

Superposition of the peptide backbone was carried out to group the 11 structures into homogenous

Table 3 $E_{pot}$ (kcal/mol) and $\langle r_{viol} \rangle$ (Å) of the 11 Structures of Peptide A Discussed in the Text

| | 1 | 2 | 3 | 4 | 5 | 6 | 7 | 8 | 9 | 10 | 11 |
|---|---|---|---|---|---|---|---|---|---|---|---|
| $E_{pot}$ (kcal/mol)(before RMD) | 251 | 240 | 232 | 238 | 242 | 250 | 234 | 251 | 243 | 247 | 241 |
| $E_{pot}$ (after RMD) | 233 | 231 | 230 | 216 | 213 | 219 | 211 | 241 | 231 | 231 | 216 |
| $\langle r_{viol} \rangle$ | 0.17 | 0.15 | 0.17 | 0.17 | 0.17 | 0.17 | 0.17 | 0.19 | 0.17 | 0.17 | 0.19 |

Table 4 Ramachandran Classification of Each of the Residues Contained in the Eleven Structures of Peptide A Obtained after DG and RMD Calculations

| | Residue *n* | | | | | | | | | | | | | | | | | |
|---|---|---|---|---|---|---|---|---|---|---|---|---|---|---|---|---|---|---|
| Structure *n* | S2 | G3 | V4 | R5 | G6 | D7 | S8 | G9 | S10 | L11 | A12 | L13 | R14 | V15 | A16 | R17 | Q18 | L19 |
| A1 | L | t″ | L | A/B | t′ | A | B | t″ | L | B | B | A | A | A | A | A | A | B |
| A2 | B | t‴ | L | A | t′ | A | B | t″ | L | B | A | A | A | A | A | A | A | B |
| A3 | B | t‴ | L | A | t′ | A | B | t″ | L | B | A | A | A | A | A | A | A | B |
| A4 | B | t′ | B | A | t′ | A | B | t″ | L | B | A | A | A | A | A | A | A | B |
| A5 | B | t′ | B | A | t′ | A | B | t″ | L | B | A | A | A | A | A | A | A | B |
| A6 | B | t′ | B | A | t′ | B | B | t″ | L | B | A | A | A | A | A | A | A | B |
| A7 | B | t′ | B | A | t′ | A | B | t″ | L | B | B | A | A | A | A | A | A | B |
| A8 | B | t′ | B | A | t′ | A | B | t′ | L | L | A | A | A | A | A | A | A | B |
| A9 | B | t‴ | L | B | t′ | A | B | t″ | L | B | A | A | A | A | A | A | A | B |
| A10 | B | t″ | L | B | t′ | A | B | t′ | L | L | A | A | A | A | A | A | A | B |
| A11 | B | t′ | B | B | t′ | A | B | t″ | L | L | B | A | A | A | A | A | A | B |

The Ramachandran classifications were expressed as H = disallowed regions, A = $\alpha$-helix, B = $\beta$-sheet. L = left-handed helix. For the Gly residues the definition were t, t′, t″ e t‴ where the latter refer to the upper left, upper right, lower left and lower right quadrant respectively of the $\phi$, $\varphi$ distribution map. The classification of each residue which contained the most favoured region of the Ramachandran plot as well as additionally allowed regions was carried out using the program PROCHECK (Lasowsky *et al.*, 1993).
The first (Gly) and last (Pro) residues of the sequence are not shown since their NMR parameters were not well defined.

Table 5 List of H-bonds Present in the 11 Selected Structures of Peptide A[a]

| H-bond (NH–CO) | Structures | | | | | | | | | | |
|---|---|---|---|---|---|---|---|---|---|---|---|
| $NH(S_2)-{}^{\delta}CO(D_7)$ | 2 | 3 | 6 | 9 | 10 | | | | | | |
| $NH(V_4)-{}^{\delta}CO(D_7)$ | 1 | 3 | 9 | 10 | | | | | | | |
| $NH(R_5)-CO(G_3)$ | 4 | 6 | 7 | 9 | | | | | | | |
| $NH_2(R_5)-{}^{\delta}CO(D_7)$ | 2 | 3 | 4 | 5 | 6 | 7 | 8 | | | | |
| $NH(D_7)-CO(A_{12})$ | 2 | 3 | 4 | 5 | 6 | 7 | 9 | | | | |
| $^{\gamma}H(S_8)-{}^{\delta}CO(D_7)$ | 1 | 2 | 3 | 4 | 5 | 7 | 8 | 11 | | | |
| $NH_2(R_{17})-CO(D_7)$ | 1 | 4 | 6 | 9 | | | | | | | |
| $NH_2(R_{17})-CO(G_6)$ | 2 | 4 | 5 | 9 | | | | | | | |
| $NH(Q_{18})-CO(V_{15})$ | 1 | 2 | 3 | 4 | 5 | 6 | 7 | 8 | 9 | 10 | 11 |
| $NH(L_{19})-CO(V_{15})$ | 1 | 2 | 3 | 4 | 5 | 6 | 7 | 8 | 10 | 11 | |

[a] Only those H-bonds found in at least four structures are indicated.

families. The first and larger family (class I) comprises structures 1, 2, 3, 4, 5, 6, 7, 9 and 11 (Figure 5A); these were very similar (backbone RMS = $1.5 \pm 0.4$ Å) although differing in some cases for either the last two residues (structure 11) or the first three residues (structures 1 and 9). Differences at both ends of the peptide were expected owing to a limited number of NOE constraints found in these regions. A second family of homogeneous models (class II) contained structures 8 and 10 (RMS = $0.8 \pm 0.2$ Å, Figure 5B).

The major difference between these two sets of structures derived from the average $\phi$ and $\psi$ angles of G9 (Table 5) which were $-100 \pm 10°$ and $-17 \pm 12°$ respectively in the first and most populated class and $123 \pm 7°$ and $78 \pm 4°$ in the second set of structures. The effects of these changes were seen in the overall shape of the models which in the case of structures 8 and 10 resembled that of a continuous irregular helix (see below) from residue 4 to residue 19 (Figure 5B).

The conformation of the residues in each structure was assigned using the Ramachandran classification (Table 4). This showed that the structure of the C-terminal half of the peptide was broadly similar in all models and was that of a helix.

The following describes in more detail the structural characteristics of individual sections of the peptide.

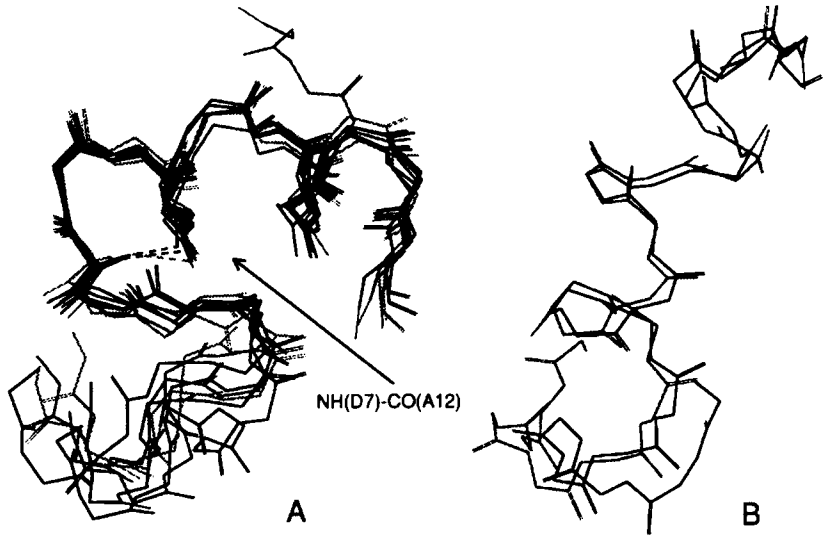


Figure 5 Backbone superposition of the two families of homogeneous structures obtained for peptide A after DG and RMD calculations. (A) structures 1, 2, 3, 4, 5, 6, 7, 9 and 11; (B) structures 8 and 10. In the case of the larger family the H-bond between D7 and A12 is shown.

***The RGDS Region.*** The backbone traces of the RGDS sequence were well superimposed in all 11 models (Figures 5 and 6). This was also evident from the Ramachandran classification of individual residues. Thus S8 was in a B($\beta$) conformation (hereafter B; see Table 4 for definition) whilst D7 and R5 were predominantly A($\alpha r$) (hereafter A) (Table 4). Analysis of the H-bond pattern (Table 5) indicated that neither the NH of D7 nor that of S8 was involved in H-bonds with preceding residues, thus ruling out, on these bases only, the existence of the $\beta$-turns and $\gamma$-turns observed in other RGDX-containing peptides [26, 27].

However, despite the absence of H-bonds, all structures clearly showed a bend around R5–G6 (Figure 6). To evaluate therefore the nature of this turn, the $O_i$–$N_{i+3}$ and $\alpha C_i$–$\alpha C_{i+3}$ distances were measured. The average value found for the $O_4$–$N_7$ distance was 6.15 Å while it was 5.5 and 8.1 Å for the $\alpha$C4–$\alpha$C7 and $\alpha$C5–$\alpha$C8 distances respectively. These values were consistent with the existence of a

Table 6 Comparison Between the $\phi$ and $\psi$ Angles of the RGD Triplet from the Two Classes of Structures of Peptide A and the X-ray Structure of $\gamma$-Crystallin II and IV

| Class[a] | Dihedral angles | R5[b] | G6[b] | D7[b] |
|---|---|---|---|---|
| I | $\phi$ | $-143 \pm 16$ | $97 \pm 19$ | $-153 \pm 12$ |
| | $\psi$ | $39 \pm 22$ | $65 \pm 10$ | $81 \pm 19$ |
| II | $\phi$ | $-65 \pm 6$ | $97 \pm 19$ | $-153 \pm 12$ |
| | $\psi$ | $-19 \pm 12$ | $65 \pm 10$ | $81 \pm 19$ |
| $\gamma$-Crystallin (II)[c] | $\phi$ | 133 | 142 | $-100$ |
| | $\psi$ | 154 | 171 | $-176$ |
| $\gamma$-Crystallin (IV)[c] | $\phi$ | $-36$ | 157 | $-124$ |
| | $\psi$ | 126 | $-167$ | $-75$ |

[a] I denotes the more abundant of the two classes of structures of peptide A (1, 2, 3, 4, 5, 6, 7, 9, and 11); II the less abundant class (structures 8 and 10).
[b] Angles are shown with their SD.
[c] Angles were extracted from the Brookhaven Data Bank.

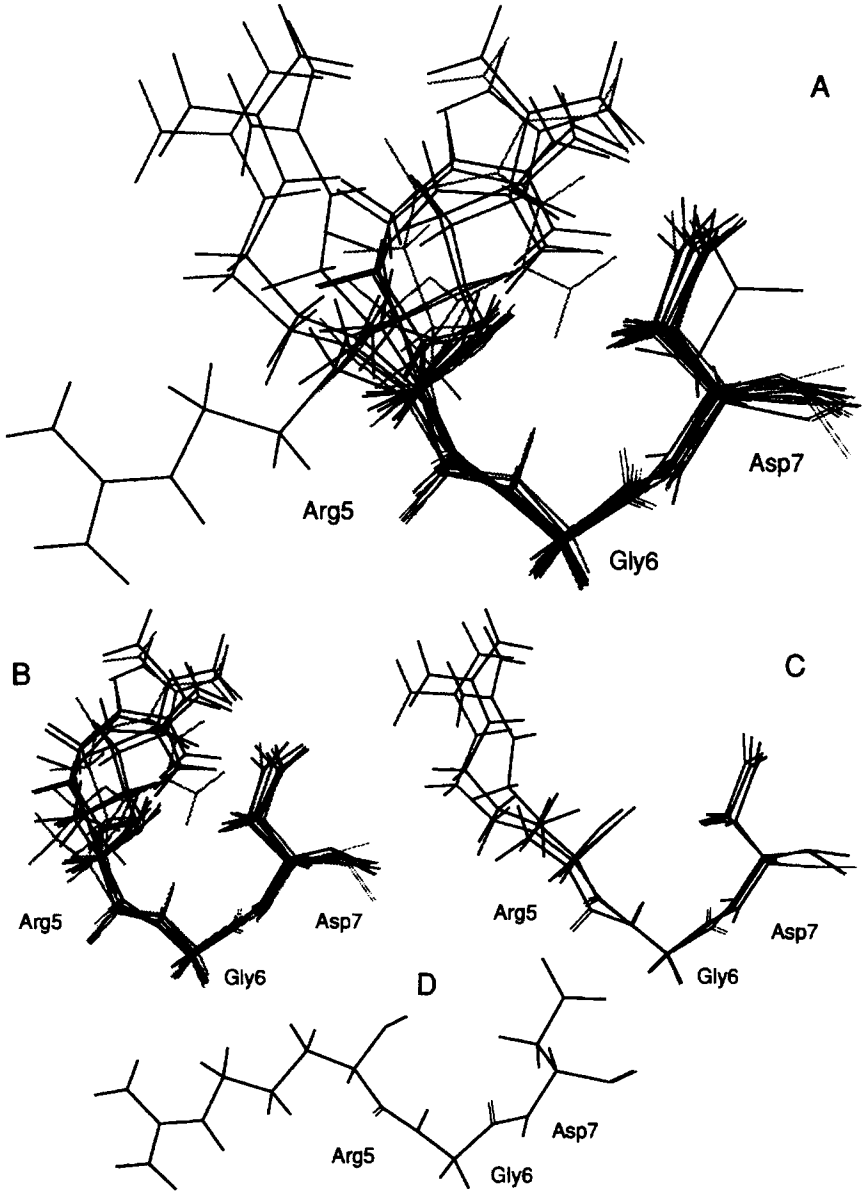


Figure 6 Superposition at the backbone of the RGD region of the 11 structures of peptide A (A). Models are grouped according to the common orientation of the side chains of R5 and D7; (B) structures 2, 3, 4, 5, 6, 7 and 8; (C) structures 1, 9 and 10; (D) structure 11.

$\beta$-turn around residues 4 to 7 which, however, did not appear to require stabilization by backbone to backbone H-bonds [29]. The dihedral angles of residues 5 and 6 (Table 6 and Figure 7) did not correspond to any of the most common $\beta$-turns [29]. The bend was therefore assigned to a type IV turn which has been defined as having two or more angles differing by at least 40° from the $\phi$ and $\psi$ values of normal $\beta$-bends and incapable of forming hydrogen bonds [30].

The type IV bend thus identified was stabilized by an interaction between the side chain of D7 and either the NH of V4 (structures 1, 3, 9 and 10) or NH-2 (structures 2, 3, 6, 9 and 10).

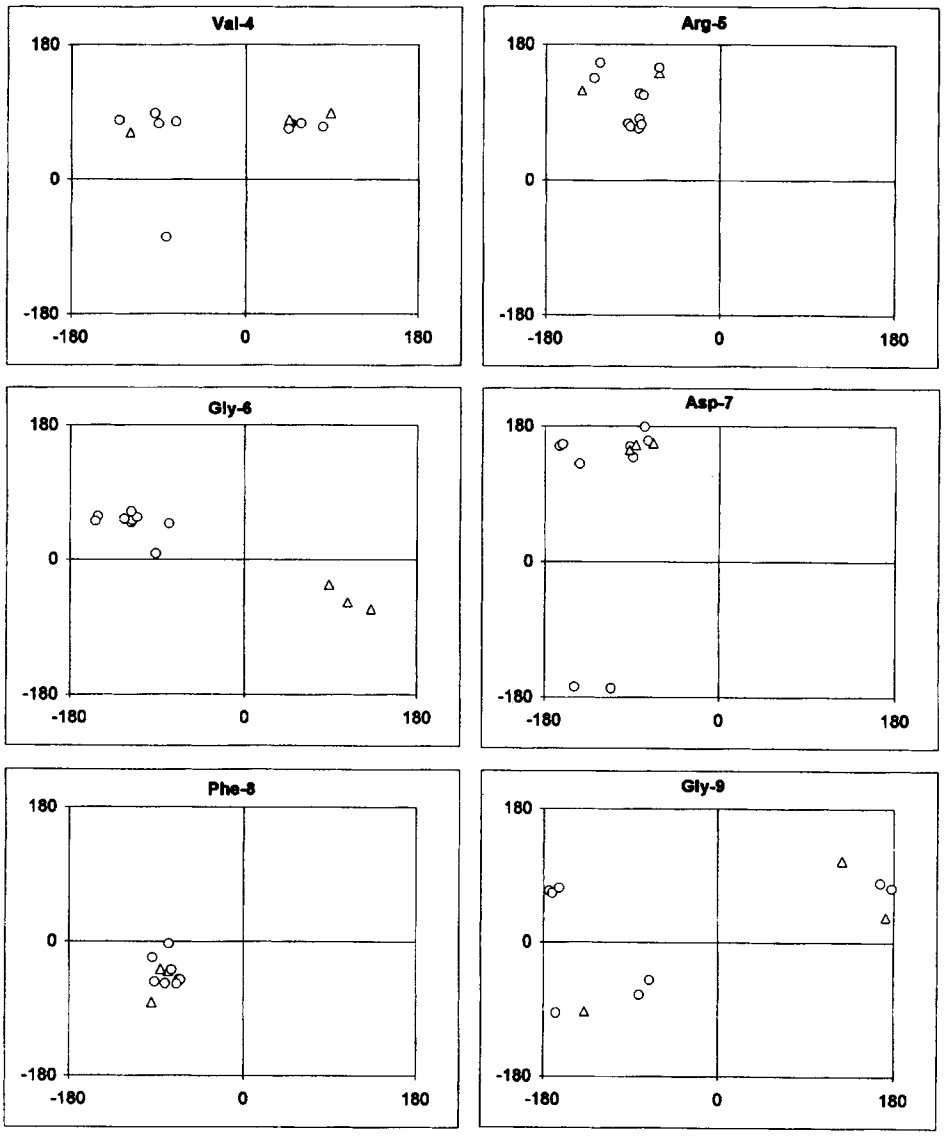


Figure 7 Distribution map of the $\phi$ and $\psi$ angles of the VRGDSG sequence of the 11 structures of peptide A. △ indicates structures 8 and 10; ○, the remaining structures.

The side chains of D7 and R5 were always on the same side of the backbone (Figure 6). H-bonds between the guanidinium and the carboxylic groups were detected in seven cases (2, 3, 4, 5, 6, 7 and 8). In three other cases (1, 9 and 10), the two side chains, although close to each other, were not within H-bonding distance. In structure 11, they pointed in opposite directions. In Figure 6 (B, C, D), the 11 models are shown incorporating the common orientations of the side chains of these two residues.

The carboxylate of D7 also formed H-bonds with the hydroxyl of S8 in all but structures 6, 9 and 10.

Collectively these results allowed us to draw a topology for the RGDS sequence whose main characteristics are as follows:

(1) The side chains of S8 and D7 are conformationally restricted and parallel to each other.
(2) The side chain of R5 is less localized although, with the exception of structure 11, close or H-bonded to the carboxyl group of D7.
(3) The three side chains are thus aligned on the same side of the backbone and accessible to solvent (Figure 8).

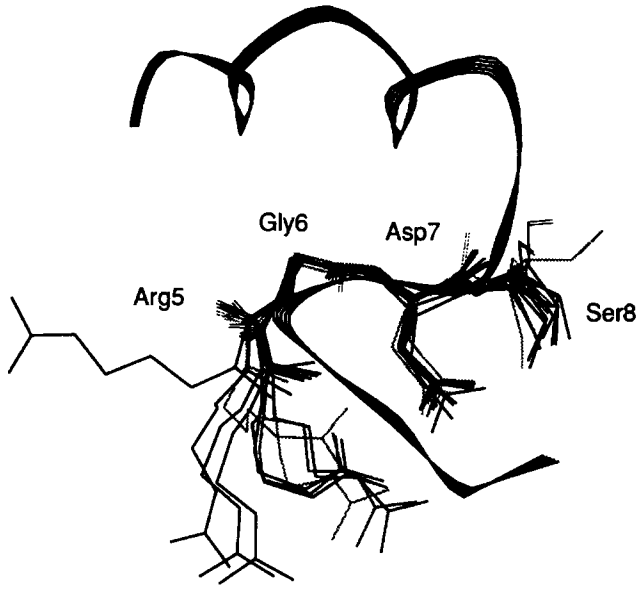


Figure 8 Relative orientation of the side chains of R5, D7 and S8 in the 11 models of peptide A. The orientation of these side chains is also shown in relation to the peptide backbone of structure 2 which was chosen as a representative model.

***The C-terminal Region.*** As indicated by the Ramachandran assignments (Table 4) the region comprising residues 12 to 18 was in a helical conformation (Figure 9). This conclusion was supported by $\alpha C_i$-$\alpha C_{i+3}$ distances which, in this region were less than 6 Å [29].

Comparison between the H-bonding pattern obtained from the NMR temperature coefficients with that extracted from the 11 models indicated consistency between the two sets of data. Thus the only two residues which in the majority of structures exhibited an H-bond were Q18 and L19 in agreement with their small temperature coefficients. It should be noticed, however, that the two H-bonds were both to the CO of

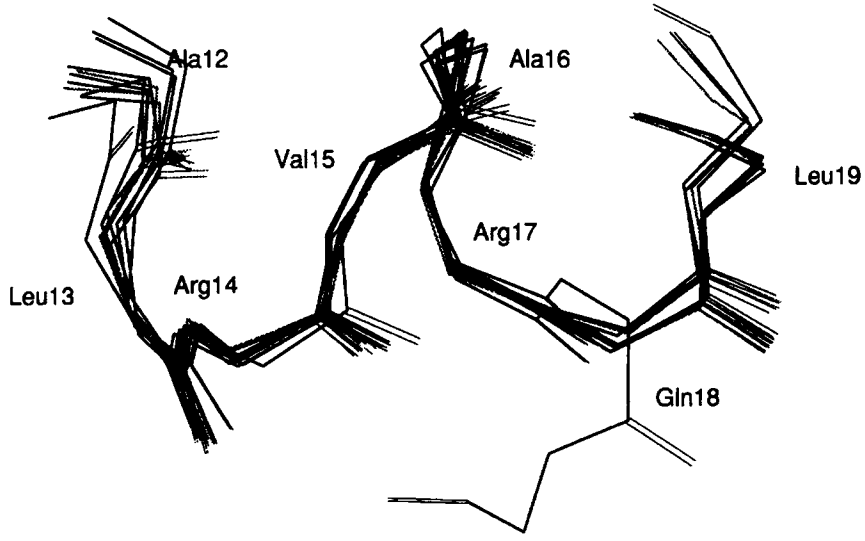


Figure 9 Backbone superimposition at the 11 structures of peptide A showing the helical character of the 12–19 region. In structure 9 a twist at the level of Q18 induces a change in the orientation of the helix.

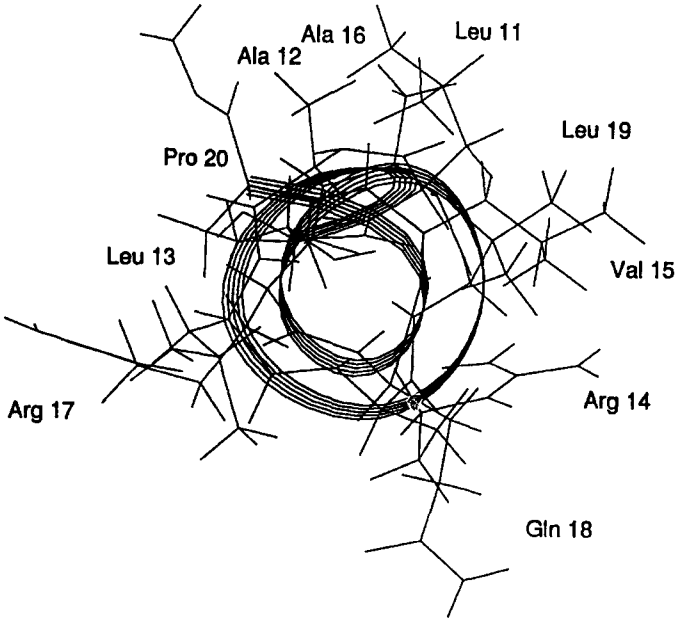


Figure 10 View of the region 11–20 along the helix axis showing the opposite orientation of hydrophobic and hydrophilic side chains typical of amphipathic helices.

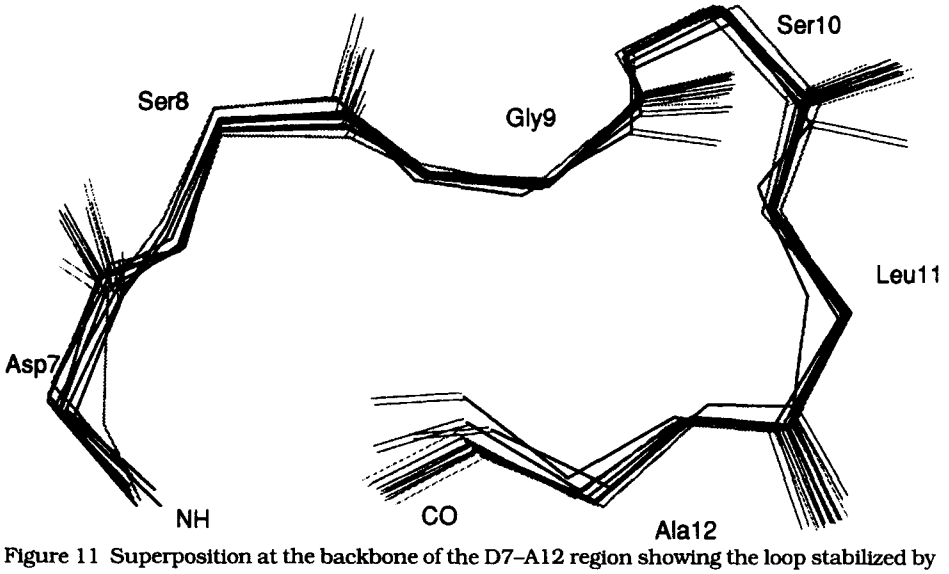


Figure 11 Superposition at the backbone of the D7–A12 region showing the loop stabilized by an H-bond between the carboxyl group of D7 and the carbonyl of A12. This loop was found in structures 1, 2, 3, 4, 5, 6, 7, 9, and 11.

V15. This and the lack of any other well-defined H-bonds in this region of the peptide did not allow the assignment of the detected helix to either $\alpha$ or $3_{10}$.

The side chains of R14 and R17 and Q18 maintained the same orientation in the two families of peptides. Their position assigned the helix to an amphipathic helix. There exist six different classes of amphipathic helixes: A, H, L. M. G and K, which differ one from another for their physicochemical properties [31]. The helical structure detected here, with a mean hydrophobic moment larger than 0.3 and a cluster of positively changed residues in the centre of the polar face, resembled an amphipathic helix type H (Figure 10) [32].

Table 7 Average Dihedral $\phi$ and $\psi$ Angles of Residues V4 and S8–L19 of the Two Classes of Structure of Peptide A Obtained After DG and RMD Calculations

| Class[a] | Dihedral Angles | V4[b] | S8[b] | G9[b] | S10[b,c] | L11[b] | A12[b] | L13[b,c] | R14[b,c] | V15[b,c] | A16[b,c] | R17[b,c] | Q18[b,c,d] | L19[b] |
|---|---|---|---|---|---|---|---|---|---|---|---|---|---|---|
| I | $\phi$ | −90±18 | −145±12 | −98±6 | 77±18 | 162±5 | −138±10 | −104±12 | −106±9 | −125±11 | −62±11 | −85±7 | −68±2 | −104±16 |
| | $\psi$ | 64±6 | 62±9 | −23±8 | 29±28 | −9±4 | 34±14 | −2±10 | −24±7 | −88±7 | 7±10 | −41±7 | −38±6 | 118±23 |
| II | $\phi$ | 47±1 | | 123±9 | | 76±6 | −124±7 | | | | | | | |
| | $\psi$ | 46±1 | | 78±6 | | 25±2 | 61±6 | | | | | | | |

[a] I denotes the more abundant of the two classes of structures; II the less abundant. See text for details.
[b] Angles are shown with their SD.
[c] Angles were the same for both classes.
[d] In structure 9 the $\phi$ and $\psi$ angles were 55° and 36° respectively.

***The Central Region.*** As discussed above the amide proton of D7 is not involved in H-bonds with preceding residues in contrast with its small NMR temperature coefficient. This apparent discrepancy was solved when the central portion of the peptide was considered. Thus with the exception of structures 8 and 10, the NH of D7 and the CO of A12 were either H-bonded or very close to each other (Figure 11). This H-bond induced a large turn (Figure 10) which was stabilized by additional interactions, those between the guanidinium group of R17 and the carbonyl of either D7 or G6. Inside this loop residues 8–10 formed a strand. In models 8 and 10, where the H-bond between D7 and A12 was absent, the additional interactions involving the side chain of R17 were also absent.

## DISCUSSION

NOE constraints combined with DG and RMD calculations were used to obtain a set of 11 structures for a peptide corresponding to the immunodominant region of FMDV serotype A. These computer-generated models were largely homogeneous and showed consistency with other NMR parameters such as temperature coefficients and $J_{N\alpha}$-coupling constants. This suggested that they might be a close representation of the solution structure of this peptide.

Superposition of the 11 structures showed that, with the exception of the less well-defined N-terminal and C-terminal residues, two families (classes I and II) of highly homogeneous structures were obtained which differed in the $\phi$ and $\psi$ angles of G9. When the latter were $-100\pm10°$ and $-17\pm12°$ (structures 1, 2, 3, 4, 5, 6, 7, 9 and 11) the peptide formed a large loop which involved residues 7 to 12 and was stabilized, in the majority of cases, by an H-bond between these two residues (Figures 5A and 11). Additional interactions between the guanidinium of R17 and the backbone carbonyls of either G6 or D7 contributed to the stabilization of this large turn. In the case of structures 8 and 10, the $\phi$ and $\psi$ angles of G8 were both positive (Table 6) , and the peptide formed a continuous irregular helical structure comprising residues 4 to 19. Thus the $\phi$ and $\psi$ angles of G9 were dependent on the D7–A12 H-bond (see Table 7). The C-terminal half of the peptide (sequence 12–19) was an amphiphatic helix in all cases (Figure 10 and Table 4).

The RGDS sequence had a topology similar in all 11 structures and independent of the backbone angles at G9. The side chains of R5, D7 and S8 were pointing in the same direction and solvent exposed in all cases. The hydroxyl group of S8 and the carboxyl group of D7 were either H-bonded or very close to each other and conformationally constrained. The side chain of R5 was less defined, although in several cases the guanidinium group was close to the carboxyl group of D7. This side-chain/side-chain interaction was important in determining the conformation of R5 since in those cases where the two residues were not in contact (structures 1, 8, 10 and 11), R5 was found to be either B or borderline between B and A (structure 1) while it was A in all other cases. $\phi$ and $\psi$ angles as well as interproton distances indicated the existence of a turn involving residues 4 to 7. This turn, which could not be classified according to any of the established and most common types of $\beta$ and $\gamma$ turns, did not apparently require stabilization through backbone–backbone H-bonds and was assigned to a $\beta$-turn type IV.

When the structural features of peptide A were compared with the X-ray structure of the G–H loop in the reduced form of the FMDV virus, serotype O [16], it was found that the general topology of the two models differed substantially. Thus, although in both cases a loop region preceded by a strand was found

around the RGD triplet, the aspartic acid at the summit of the loop in the X-ray structure was replaced by glycine in the models presented here. Furthermore the helical region, which in the reduced form of the virus follows the aspartic acid, was replaced, in the majority of the eleven models of peptide A, by a short, extended strand comprising residues 8 to 10. Confirmation of the differences between the two models was obtained from the comparison of the dihedral angles of peptide A with those of $\gamma$-crystallin which, when superimposed on the X-ray structure of the RGD triplet had been found to give an RMS deviation of 0.09 Å [6]. None of the models for peptide A had, in the RGD region, $\phi$ and $\psi$ angles consistent with those of the protein (Table 6). Possible explanations to these differences were as follows.

Firstly the peptide analysed here and the published viral structure are from two different serotypes and structural differences at the level of the G–H loop are expected given the lack of cross-reactivity between the two serotypes in serological tests [33]. Secondly, our model could represent the conformation adopted by the peptide when interacting with antibodies while the published X-ray structure could reflect the conformational features needed for receptor binding. Support for this hypothesis came from (1) the serological data on the reduced virus which indicated that whilst the virus was still partly infectious, the ability of antiserum to the G–H loop peptide to distinguish between the parent and the reduced form of the virus was abolished [34] and (2) the different conformational features found for peptide A and USA (see accompanying paper) which suggest that the proposed models are a more likely explanation for their different serological behaviour rather than reflecting an obviously similar conformational state necessary for cell entry.

### Notes added in proof

During the course of revision of this work a manuscript was published which describes the X-ray crystal structure of a peptide corresponding to the major antigenic loop of FMDV, serotype C, complexed with a neutralising antibody (55).

In this complex the RGD triplet shows the same open turn conformation found in the reduced form of FMDV serotype D (6).

This finding suggests that the differences found between our peptide and those from serotypes O and C may derive mainly from structural differences at the level of the G–H loop.

### Acknowledgements

This work has been supported by the Wellcome Trust (grant no. 18937/1.5). L. Z. and H. M. have been supported by the 'Progetto Finalizzato Chimica Fine e Secondaria' (sottoprogetto 3.2) of the Italian CNR and are indebted to F. Greco for technical assistance. M. P. has been supported by Italfarmaco spa, Milan, Italy.

## REFERENCES

1. J. L. Bittle, R. A. Houghten, H. Alexander, T. M. Shinnick J. G. Sutcliffe, R. A. Lerner, D. J. Rowlands and F. Brown (1982). Protection against foot-and-mouth disease by immunisation with a chemically synthesised peptide predicted from the viral nucleotide sequence. *Nature, 298*, 30–33.
2. G. Fox, N. R. Parry, P. V. Barnett, B. McGinn, D. J. Rowlands and F. Brown (1989). The cell attachment site on foot-and-mouth disease virus includes the amino acid sequence RGD (arginine–glycine–aspartic acid). *J. Gen. Virol., 70*, 625–637.
3. N. R. Parry, E. J. Ouldridge, P. V. Barnett, B. E. Clarke, M. J. Francis, J. D. Fox, D. J. Rowlands and F. Brown (1989). Serological prospects for peptide vaccines against foot-and-mouth disease virus. *J. Gen. Virol. 70*, 2919–2932.
4. L. Acharya, E. Foy, D. Smart, G. Fox, D. Rowlands and F. Brown (1989). The three-dimensional structure of foot-and-mouth disease virus at 2.9 Å resolution. *Nature, 337*, 709–711.
5. S. Lea, J. Hernandez, W. Blakemore, E. Brocchi, S. Curry, E. Domingo, E. Fry, R. Abu-Ghazaleh, A. King, J. Newman, D. Stuart and M. G. Mateu (1994). The structure and antigenicity of a type C foot-and-mouth disease virus. *Structure, 2*, 123–139.
6. D. Logan, R. Abu-Ghazaleh, W. Blakemore, S. Curry, T. Jackson, A. King, S. Lea, R. Lewis, J. Newman, N. Parry, D. Rowlands, D. Stuart and E. Fry (1993). Structure of a major immunogenic site of foot-and-mouth disease virus. *Nature, 362*, 566–567.
7. D. J. Rowlands, B. E. Clark, A. R. Carrol, F. Brown, B. H. Nicholson, J. L. Bittle, R. A. Houghten and R. A. Lerner (1983). Chemical basis of antigenic variation in foot-and-mouth disease virus. *Nature, 306*, 694–697.
8. G. Siligardi, A. F. Drake, P. Mascagni, D. Rowlands, F. Brown and W. A. Gibbons (1991). A CD strategy for the study of polypeptide folding/unfolding. A synthetic foot-and-mouth disease virus immunogenic peptide. *Int. J Peptide Protein Res., 38*, 519–527.
9. G. Siligardi, A. F. Drake, P. Mascagni, D. Rowlands, F. Brown and W. A. Gibbons (1991b). Correlation between the conformations elucidated by CD spectroscopy and the antigenic properties of four peptides of the foot-and-mouth disease virus. *Eur. J. Biochem., 199*, 545–551.
10. H. J. Dyson, G. Merutka, J. P. Waltho, R. A. Lerner and

P. E. Wright (1992) Folding of peptide fragments comprising the complete sequence of proteins. Models for initiation of protein folding I Myohemerythrin. *J. Mol. Biol.*, *226*, 795–817.

11. H. J. Dyson, J. R. Sayre, G. Merutka, H. C. Shin, R. A. Lerner and P. E. Wright (1992). Folding of peptide fragments comprising the complete sequence of proteins. Models for initiation of protein folding I Plastocyanin. *J. Mol. Biol.*, *226*, 819–835.
12. D. Sonnichsen, J. E. Van Eyk, R. S. Hodges and B. D. Sykes (1992). Effect of trifluoroethanol on protein secondary structure: an NMR and CD study using a synthetic actin peptide. *Biochemistry*, *31*, 8790–8798.
13. A. Jasonoff and A. R. Fersht (1994). Quantitative determination of helical propensity from TFE titration curves. *Biochemistry*, *33*, 2129–2135.
14. D. K. Waterhouse and W. C. Johnson Jr (1994). Importance of environment in determining secondary structure in proteins. *Biochemistry*, *33*, 2121–2128.
15. L. L. France, P. G. Piatti, J. F. E. Newman, I. Toth, W. A. Gibbons and F. Brown (1994). Circular dichroism, molecular modeling and serology indicate that the structural basis of antigenic variation in foot-and-mouth disease virus is $\alpha$-helix formation. *Proc. Natl Acad. Sci. USA*, *91*, 8442–8446.
16. C. Griesinger, G. Otting, K. Wuethrich and R. R. Ernst (1988) Clean TOCSY for $^1$H spin system identification in macromolecules. *J. Am. Chem. Soc.*, *110*, 7870–7872.
17. T. F. Havel, J. D. Kuntz and G. M. Crippen (1983). The theory and practice of distance geometry. *Bull. Math. Biol* *45*, 655–720.
18. T. F. Havel and K. Wütrich (1984). A distance geometry program for determining the structures of small proteins and other macromolecules from nuclear magnetic resonance measurements of intramolecular $^1$H–$^1$H proximities in solution. *Bull. Math. Biol.*, *46*, 673–698.
19. R. Fletcher and C. M. Reeves (1964). Function minimization by conjugate gradients. *Comput. J.*, *7*, 149–167.
20. G. M. Clore, A. M. Gronenborg, A. T. Brünger and M. Karplus (1985). Solution conformation of a heptadecapeptide comprising the DNA binding helix F of the cyclic AMP receptor protein of *Escherichia coli*. Combined use of $^1$H nuclear magnetic resonance and restrained molecular dynamics. *J. Mol. Biol.*, *186*, 435–455.
21. R. Kaptein, E. R. P. Zuiderberg, R. M. Scheek, R. Boelens and W. F. van Gunsteren (1985). A protein structure from nuclear magnetic resonance data of lac repressor headpiece. *J. Mol. Biol.*, *182*, 179–182.
22. J. de Vlieg, R. M. Scheek, W. F. van Gunsteren, H. J. C. Berendsen, R. Kaptein and J. Thomason (1988). Combined procedure of distance geometry and restrained molecular dynamics techniques for protein structure determination from nuclear magnetic resonance data: application to the DNA binding domain of lac repressor from *Escherichia coli*. *Proteins: Struct. Funct. Genet.*, *3*, 209–218.
23. K. Wuethrich: *NMR of Proteins and Nucleic Acids*, Wiley, New York 1986.
24. G. Esposito and A. Pastore (1988). An alternative method for distance evaluation from NOESY spectra. *J. Magn. Reson.*, *76*, 331–336.
25. G. C. Johnson Jr, T. G. Pagano, C. T. Basson, J. A. Madri, P. Gooley and I. M. Armitage (1993). Biologically active Arg-Gly-Asp oligopeptides assume a type II $\beta$-turn in solution. *Biochemistry*, *32*, 268–273.
26. M. J. Bogusky, A. M. Naylor, S. M. Pitzenberger, R. F Nutt, S. F. Brady, C. D. Colton, J. T. Sisko, P. S. Anderson and D. F. Veber (1992). NMR and molecular modeling characterization of RGD containing peptides. *Int. J. Peptide Proteins Res.*, *39*, 63–76.
27. M. C. Vega, C. Aleman, E. Giralt and J. J. Perez (1992). Conformational study of a nine residue fragment of the antigenic loop of foot-and-mouth disease virus. *J. Biomol. Struct. Dynamics*, *10*, 1–8.
28. W. Braun (1987). Distance geometry and related methods for protein structure determination from NMR data. *Q. Rev. Biophys.*, *19*, 115–157.
29. P. Y. Chou and G. D. Fasman (1977). $\beta$-turn in proteins. *J. Mol. Biol.*, *115*, 135–175.
30. D. J. Rowlands, B. E. Clark, A. R. Carrol, F. Brown, B. H. Nicholson, J. L. Bittle, R. A. Houghten and R. A. Lerner (1983). Chemical basis of antigenic variation in foot-and-mouth disease virus. *Nature*, *306*, 694–697.
31. J. P. Segrest, H. De Loof, J. G. Dohlman, C. G. Brouillette and G. M. Anantharamaiah (1990). Amphiphatic helix motif: classes and properties. *Proteins: Struct. Funct. Genet.*, *8*, 103–117.
32. D. Eisenberg, E. Schwartz, M. Komaramy and R. Wall (1984). Analysis of membrane and surface protein sequences with the hydrophobic moment plot. *J. Mol. Biol.*, *179*, 125–142.
33. N. R. Parry, P. V. Barnett, E. J. Ouldridge, D. J. Rowlands and F. Brown (1989). Neutralizing epitopes of type O foot-and-mouth disease virus. II. Mapping three conformational sites with synthetic peptide reagents. *J. Gen. Virol.*, *70*, 1493–1503.
34. N. P. Parry, G. Fox, D. Rowlands, F. Brown, E. Fry, R. Acharya, D. Logan and D. Stuart (1990). Structural and serological evidence for a novel mechanism of antigenic variation in foot and mouth disease virus. *Nature*, *347*, 569–572.
35. N. Verdaguer, M. G. Mateu, D. Andreu, E. Giralt, E. Domingo and I. Fita (1995) Structure of the major antigenic loop of FMDV complexed with a neutralising antibody: direct involvement of the RGD motif in the interaction. *EMBO J.*, **14**, 1690–1696.